Pedestal structure and inter-ELM evolution for different main ion species in ASDEX Upgrade

F. M. Laggner,[1, a)] E. Wolfrum,[2] M. Cavedon,[2,3] F. Mink,[2,3] M. Bernert,[2] M. G. Dunne,[2] P. A. Schneider,[2] A. Kappatou,[2] G. Birkenmeier,[2,3] R. Fischer,[2] M. Willensdorfer,[2] F. Aumayr,[1] the EUROfusion MST1 Team,[b)] and the ASDEX Upgrade Team

[1)] *Institute of Applied Physics, TU Wien, Fusion@ÖAW, Wiedner Hauptstr. 8-10, 1040 Vienna, Austria*

[2)] *Max Planck Institute for Plasma Physics, Boltzmannstr. 2, 85748 Garching, Germany*

[3)] *Physik-Department E28, Technische Universität München, James-Franck-Str. 1, 85748 Garching, Germany*

(Dated: 22 December 2016)

In tokamak plasmas with different main ion species a change of confinement occurs, known as isotope effect. Experiments comparing hydrogen (H), deuterium (D) and helium (^{4}He) plasmas have been performed to identify processes that define the pedestal structure and evolution in between the crashes of edge localized modes (ELMs). The pedestal top electron densities and temperatures have been matched to compare the pedestal shape and stability. In the D and H discharges the pedestal electron temperature profiles do not differ, whereas the density profile in H has shallower gradients. Furthermore, the heat flux across the pedestal in H is roughly a factor of two higher than in D. In ^{4}He plasmas at similar stored energy the pedestal top electron density is roughly a factor of 1.5 larger than in the references owing to the larger effective charge. Peeling-ballooning theory, which is independent of the main ion species mass, can sufficiently describe the pedestal stability in the hydrogenic plasmas. The inter-ELM pedestal evolution has the same sequence of recovery phases for all investigated species, giving evidence that similar mechanisms are acting in the pedestals. This is further supported by a similar evolution of the inter-ELM magnetic signature as well as corresponding toroidal structure.

PACS numbers: 52.55.-s, 52.55.Fa, 52.55.Tn
Keywords: Plasma, Tokamak, ELM

[a)]Electronic mail: laggner@iap.tuwien.ac.at

[b)]See the author list of "Overview of progress in European Medium Sized Tokamaks towards an integrated plasma-edge/wall solution" by H. Meyer et al., to be published in Nuclear Fusion Special issue: Overview and Summary Reports from the 26th Fusion Energy Conference (Kyoto, Japan, 17-22 October 2016)

I. INTRODUCTION

The next step fusion experiment, ITER, will start its operation with either hydrogen (H) or more likely helium (^{4}He) plasmas to commission the operationally relevant systems and plasma diagnostics in a non-nuclear environment and develop plasma scenarios for deuterium-tritium (D-T) operation[1]. The foreseen plasma scenario is the high confinement mode (H-mode), which is characterized by an edge transport barrier (ETB) and connected to steep gradients in the temperature, density and consequently in the pressure at the plasma edge, called pedestal. The origin of the ETB is a radially sheared E × B flow, caused by the radial electric field (E_r), which reduces the turbulent transport due to decorrelation of the turbulent eddies[2,3]. To achieve the transition from low confinement mode (L-mode) to H-mode the L-H power threshold ($P_\mathrm{L-H}$), has to be exceeded[4]. This $P_\mathrm{L-H}$ differs when exchanging the main ion species of the plasma[5]. It has been found that the edge ion heat flux at the L-H transition is about twice as high in H as in deuterium (D) plasmas[6] at similar ion temperature gradient (∇T_i). The latter suggests that in both plasmas E_r at the L-H transition is similar.

Similar to the difference in $P_\mathrm{L-H}$, better plasma confinement for heavier hydrogenic isotopes has been experimentally observed in H-mode[7,8]. This behaviour is contrary to the expected confinement assuming gyro-Bohm diffusive transport because the gyro radius increases with mass at fixed temperature. The worse energy confinement in H H-mode plasmas was attributed to enlarged core heat conductivity[9]. Also losses due to edge localized modes (ELMs) and the pedestal can have a significant contribution to the plasma stored energy (W_MHD)[10]. The behaviour of ELMs, in terms of ELM frequency (f_ELM), particle and energy losses, has been reported to change, when different main ion species are investigated[11] especially in ^{4}He plasmas[12,13]. With respect to ITER's non-nuclear operation one important question is if the behaviour of H or ^{4}He plasmas can be extrapolated to scenarios for D-T operation.

Usually core, edge and effects caused by ELMs are coupled[14,15], this paper focuses on their separation and ordering in plasmas with different main ion species. For this reason, the pedestal top electron density (n_e) and electron temperature (T_e) in D, H and ^{4}He plasmas were matched. Using the plasma edge diagnostics with high spatial as well as temporal resolution at ASDEX Upgrade[16], the pedestal structure, stability and inter-ELM evolution

are characterized.

The paper is organized as follows: The experimental procedure is motivated and an introduction to the utilized data analysis methods is presented in Section II. The pedestals of hydrogenic species plasmas (D,H) are compared to linear ideal magnetohydrodynamic (MHD) stability analysis and the inter-ELM evolution is characterized in Section III. Section IV shows pedestal structure and inter-ELM evolution of ^{4}He plasmas. Finally, the results are summarized in Section V giving a consistent picture: peeling-ballooning (PB) theory consistently describes the pedestal stability for the investigated cases of hydrogenic species. ELM behaviour and pedestal structure for different main ion species can be explained by the necessary variation of control parameters. There seems to be no difference in the pedestal dynamics, magnetic signature and corresponding structure of inter-ELM magnetic fluctuations, indicating no change of the dominant processes by exchange of the main plasma isotope.

II. EXPERIMENTAL MOTIVATION AND SETUP

The conducted experiments aim at a quantitative comparison of pedestals in plasmas with different main ion species. A match of the pedestal n_e, T_e and ion temperature (T_i) was performed keeping the magnetic configuration; toroidal magnetic field (B_t), plasma current (I_p) and plasma shape. The chosen plasma scenario was a lower single null discharge with $I_\mathrm{p} = 1.0\,\mathrm{MA}$, $B_\mathrm{t} = -2.5\,\mathrm{T}$ (negative sign stands for opposite direction to I_p) at an average triangularity of 0.22. The varied control parameters were heating power (P_heat) and the gas puff. This procedure enables a direct comparison of the edge stability between the different ion species. The ELM behaviour (frequency, losses and temporal evolution) with similar pre-ELM pedestal structure can be directly compared and the inter-ELM magnetic activity is characterized.

The pedestal profiles are measured by the following diagnostics: The n_e profile is measured by lithium beam emission spectroscopy[17] at the edge and by deuterium cyanide laser interferometry[18] in the core. The T_e profile is reconstructed from electron cyclotron emission (ECE)[19]. Within the integrated data analysis framework[20] the information of these diagnostics is combined to evaluate the best fits of n_e and T_e (parameterized by cubic splines). Here, a forward modelling of the electron cyclotron radiation transport[21] is ap-

plied to reliably determine the T_e profile at the pedestal and around the separatrix in the optically thin plasma. The T_e profile is radially shifted such that a separatrix T_e of 100 eV is matched[16]. Relative alignment of the n_e and T_e profiles is cross checked with the Thomson scattering diagnostic[22], which measures both quantities simultaneously at the same position. To achieve these conditions, generally shifts smaller than 3 mm are applied. The later presented n_e and T_e profiles are analyzed with a temporal resolution of 250 μs.

The presented T_i profiles are measured by the edge charge exchange recombination spectroscopy (CXRS) system[23] with a temporal resolution of 2.3 ms. The radial resolution is 3 mm at the edge and increases towards the pedestal top to roughly 5 mm. Typically, the CXRS diagnostic employs charge exchange between low charge number impurities, e.g. boron or nitrogen, and injected neutrals. In the case of ^{4}He plasmas the main ions can be directly investigated. A recent upgrade of the spectrometer[24] enables a temporal resolution down to 70 μs enabling the study of the inter-ELM evolution of T_i.

III. COMPARISON OF HYDROGENIC MAIN ION SPECIES

A. Pedestal structure and stability

By a variation of two control parameters, gas puff and P_{heat}, a match of T_e as well as reasonable agreement of T_i pedestal profiles (pedestal top T_i slightly higher in H) are achieved (see Fig. 1, blue: D, red: H). Due to a different electron density gradient (∇n_e) it is only possible to match the pedestal top n_e (Fig. 1 a). This pedestal top match required roughly a factor of 2 higher heating power (D: P_{heat} 3.9 MW, H: P_{heat} 7.5 MW) as well as a factor of almost 10 higher gas puff (D: $1.5 \cdot 10^{21}$ e/s, H: $12.1 \cdot 10^{21}$ e/s) in the H plasma. The heating systems were electron cyclotron resonance heating (ECRH) at central deposition location to avoid impurity accumulation (1.1 MW in both plasmas) and neutral beam injection (NBI) operated with the particular ion species. The shallower ∇n_e in the H plasma is probably caused by the change of particle confinement. A stronger ionization source in H due to the higher gas puff, located further inside the plasma because of the faster velocity of neutrals, would lead to higher pedestal top n_e at similar particle confinement.

To compare the stability of both plasmas and investigate the impact of the shallower ∇n_e, linear MHD stability analysis is performed using the recently improved stability workflow

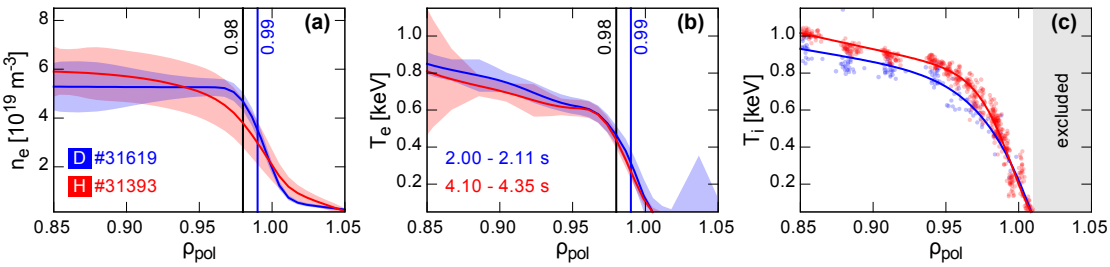

FIG. 1: Pre-ELM (averaged between −2.0 and −1.0 ms relative to the ELM onset) profiles of (a) n_e, (b) T_e and (c) T_i for D (blue) and H (red). The coloured vertical bars indicate radial positions at which the inter-ELM temporal evolution of the corresponding quantities are tracked in Fig. 4. The gradient of the n_e profile in H is shallower than in D, leading to a wider pedestal and a reduction of the achievable pressure gradient (compare Fig. 2).

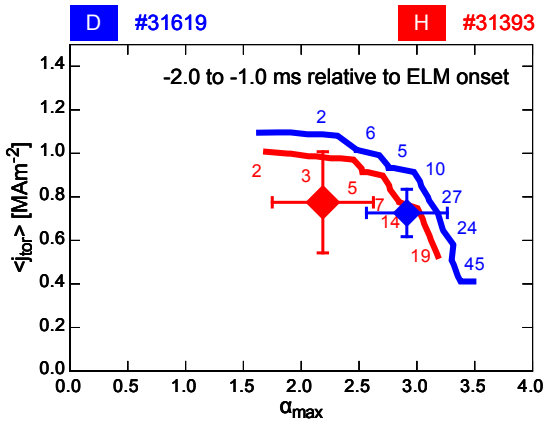

FIG. 2: Comparison of the pre-ELM stability boundaries (determined between −2 and −1 ms relative to the ELM onset) for the D (blue) and the H (red) plasma: average toroidal current density in the pedestal ($\langle j_{tor} \rangle$) and maximum normalized pressure gradient (α_{max}). Both operational points are located close to the PB part of the boundary.

at ASDEX Upgrade[25]. As input served a pressure constrained magnetic equilibrium that includes the reconstructed edge current density[26]. The resulting boundaries and corresponding operational points are presented in Fig. 2 in terms of average toroidal current density in the pedestal ($\langle j_{tor} \rangle$) and maximum normalized pressure gradient (α_{max}). Owing to the shallower ∇n_e in H, α_{max} is lower, leading to a reduced operational point in α_{max}. Within the experimental uncertainties both plasmas are qualitatively consistent with PB theory. This suggests that the pedestal stability is not affected by the main ion species and simply

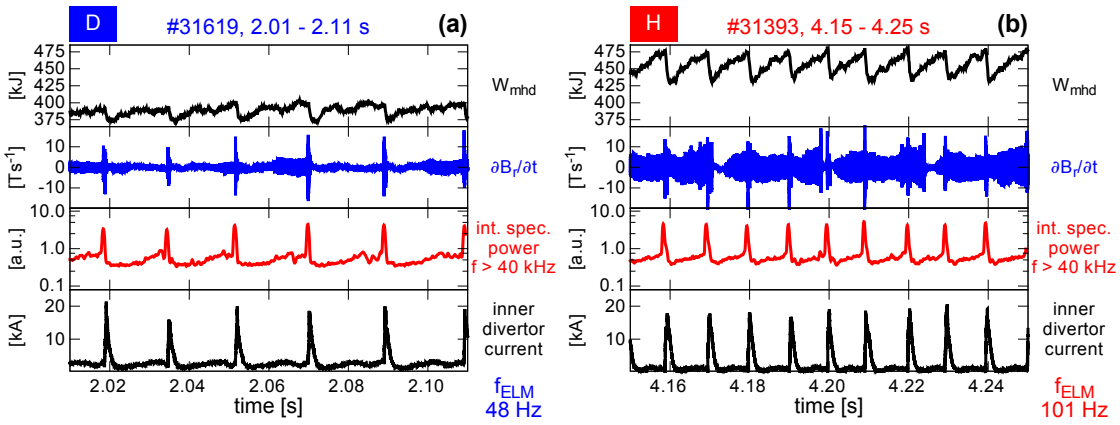

FIG. 3: Time traces of 100 ms duration of the (a) D and (b) H plasma discharge: plasma stored energy (W_{MHD}, black, top plot), radial magnetic field fluctuations ($\partial B_{\mathrm{r}}/\partial t$, blue), the integrated spectral power of $\partial B_{\mathrm{r}}/\partial t$ for frequencies larger than 40 kHz (red) and divertor shunt current (black, bottom plot). The f_{ELM} in the H plasma is about twice as large as in the D plasma and the W_{MHD} losses due to ELMs are larger in H.

determined by the plasma edge profiles.

B. ELM behaviour and losses

The evolution in between ELM crashes is compared using the time traces presented in Fig. 3 for D and H. The plasma stored energy (W_{MHD}), radial magnetic field fluctuations ($\partial B_{\mathrm{r}}/\partial t$) measured by a magnetic pickup coil that is located at the low field side (LFS) midplane (B31-14), the integrated spectral power of $\partial B_{\mathrm{r}}/\partial t$ (for frequencies larger than 40 kHz) and divertor current, measured by shunts in the divertor target plates (bursts indicate the ELM crashes), are plotted. By counting the number of ELMs (since the chosen time intervals have similar length), it is visible that the f_{ELM} is about twice as large in the H plasma in comparison to the D plasma. A list of further ELM characterizing quantities and their uncertainties can be found in Table I. In terms of average ELM energy losses (ΔW_{MHD}) the ELMs in H are almost twice as large as in D. But the W_{MHD} before the ELM crash is about 20 % higher in H because of slightly higher n_{e} and T_{i} from the pedestal inwards (compare Fig. 1) and likely a larger amount of fast-ions since the heating power from NBI is higher. In principle the larger stored energy should be beneficial for the pedestal stability due to a bigger Shafranov shift. However, it can be seen in Fig. 2 this effect is overruled by

species	shot	f_{ELM} [Hz]	ΔW_{MHD} [kJ]	ΔW_{MHD} [%]	P_{ELM} [MW]	P_{heat} [MW]	P_{net} [MW]	$P_{\mathrm{rad,sep}}$ [MW]	$\frac{P_{\mathrm{ELM}}}{P_{\mathrm{net}}-P_{\mathrm{rad,sep}}}$ [%]
D	#31619	48 ± 17	20.1 ± 4.6	5.1 ± 1.2	0.97 ± 0.41	3.93	3.76	1.25 ± 0.15	38.6 ± 16.5
H	#31393	101 ± 6	36.9 ± 5.2	7.9 ± 1.1	3.73 ± 0.97	7.51	7.28	0.72 ± 0.22	56.8 ± 8.9

TABLE I: ELM energy and power losses for D and H: ELM frequency (f_{ELM}), average ELM energy loss (ΔW_{MHD}), power loss by ELMs (P_{ELM}), heating power (P_{heat}), corrected heating power (P_{net}), radiated power inside the separatrix ($P_{\mathrm{rad,sep}}$) and relative power loss by ELMs [$P_{\mathrm{ELM}}/(P_{\mathrm{net}} - P_{\mathrm{rad,sep}})$]. In both species about half of power crossing the separatrix is transported by ELMs. In absolute numbers an enhanced heat flux across the pedestal in H is required to balance the power.

the shallower ∇n_{e} and only of secondary order in this comparison.

Taking into account the differences in W_{MHD}, the average relative ELM energy losses are approximately 1.5 times higher in H in comparison to D. Combining f_{ELM} and ΔW_{MHD}, the power losses caused by ELMs (P_{ELM}) in H are about 4 times the one in D. The relative power losses caused by ELMs [$P_{\mathrm{ELM}}/(P_{\mathrm{net}} - P_{\mathrm{rad,sep}})$] are calculated using the for beam losses and $\partial W_{\mathrm{MHD}}/\partial t$ corrected heating power (P_{net}) and the radiated power inside the separatrix ($P_{\mathrm{rad,sep}}$). These are in the range of about 40 to 50 % in both plasmas. In D, $P_{\mathrm{rad,sep}}$ is 1.8 times larger than in H, because of a higher tungsten concentration since low gas puff and low heating power were applied. To fulfill power balance the remaining power $P_{\mathrm{net}} - P_{\mathrm{rad,sep}} - P_{\mathrm{ELM}}$ has to be lost by heat transport. Therefore, a factor of 1.8 higher heat flux across the pedestal is required in H in comparison to D.

An indicator for the presence of instabilities or modes in the plasma are fluctuations of the magnetic field. In between the ELM crashes, the detected $\partial B_{\mathrm{r}}/\partial t$ (Fig. 3, blue) is larger in amplitude for H than for D. This is mainly caused by a larger amplitude response of a core mode in the H plasma, which dominates the power in frequencies up to 40 kHz. The inter-ELM integrated spectral power for frequencies larger than 40 kHz (red) is at similar levels for both main ion species. Furthermore, the integrated spectral power shows a similar evolution. After the ELM crash a phase of low fluctuation level, correlated to the n_{e} pedestal recovery (see Section III C), is observed. This phase is followed by an increase (during the T_{e} pedestal recovery), resulting in a saturated phase before the ELM onset, in which it has been found that the maximum pedestal gradients are clamped[27]. The toroidal structure of these fluctuations is analyzed in more detail in Section III D.

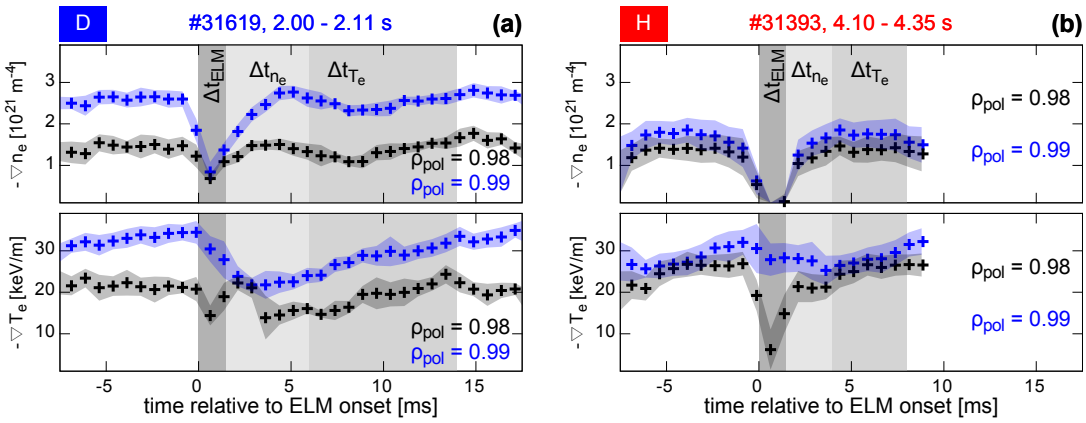

FIG. 4: Pedestal gradient evolution throughout the ELM cycle: ∇n_e and ∇T_e at certain positions (ρ_{pol} ; compare Fig. 1) for the (a) D and (b) H plasma. The pedestal recovery phases have a similar sequence in both main ion species but different duration (Δt_{n_e}, Δt_{T_e}).

C. Inter-ELM pedestal evolution

Comparing the inter-ELM evolution of the pedestal n_e and T_e for the different ion species gives insight in the build-up of the pre-ELM pedestal structure. It has been found previously in D plasmas that the n_e pedestal recovers on a shorter timescale than the T_e pedestal[28]. A change of this behaviour in H would be a strong indication for different mechanisms acting on the pedestal. In Fig. 4 the ELM synchronized evolution of ∇n_e and electron temperature gradient (∇T_e) for D and H at representative radial locations ($\rho_\mathrm{pol} = 0.98$ and 0.99), which are also indicated in Fig. 1, are presented. In both main ion species the pedestal shows qualitatively similar recovery phases, i.e. the pedestal n_e recovers faster than the pedestal T_e.

The first phase in the ELM-cycle is the ELM crash, which has a duration Δt_ELM of 1.5 ms for both plasmas, according to the duration of the bursts in the divertor shunt current. This phase is followed by the recovery of the n_e pedestal with duration Δt_{n_e}, which is longer in D. Two possible mechanisms could cause this difference in Δt_{n_e}: On the one hand the 10 times higher gas puff (larger particle source) as well as the faster velocity of recycled particles due to the lower mass in H or on the other hand an increased outward particle transport from the core to the pedestal top in H. The third phase is the recovery of the T_e pedestal, respectively ∇T_e. Here, the duration Δt_{T_e} is also longer in D, most probably caused by the lower heat flux to the pedestal. During the last phase of the ELM cycle the pedestal

gradients do not evolve and high frequency magnetic fluctuations set in (see Section III D). This period lasts up to several milliseconds in D, whereas in H it is just present for 1 to 2 ms. Qualitatively, a similar sequence of pedestal recovery phases is observed in D and H.

D. Structure of pre-ELM magnetic fluctuations

Analyzing the toroidal structure of magnetic fluctuations can give further insight in the underlying instabilities causing them. Furthermore, comparing the frequencies of the detected $\partial B_\mathrm{r}/\partial t$ enables the determination of propagation velocities of the structures.

To measure the toroidal mode structure a toroidal array of magnetic pickup coils is installed in ASDEX Upgrade. Analyzing the relative phase shifts (and multiples of 2π added/subtracted) in between the coils signals, one can determine the toroidal structure of the detected fluctuations, represented by the toroidal mode number (n). It is important to consider that the pickup coils can have an intrinsic, frequency dependent phase response (due to inductances or shielding), especially at higher frequencies. For this reason, these intrinsic phases have to be taken into account for a reliable n determination[29]. Recently, the method has been improved by statistically increasing the amount of data using ELM synchronization[30], which enables the analysis of n throughout the ELM cycle.

To compare the frequency resolved magnetic activity at the LFS midplane for the hydrogenic species, Figs. 5 a and 5 c present ELM synchronized frequency histograms for D and H. At lower frequencies (< 40 kHz) the frequency histogram is dominated by a core mode in both presented cases. The post-ELM magnetic activity in the medium frequency range (40 to 200 kHz) during the n_e pedestal recovery (Δt_{n_e}, Fig. 4) is lower than in the other phases of the pedestal evolution. In D the fluctuations in this frequency range are more band-like than in H, where they are rather broadband. After the recovery of the T_e pedestal (Δt_{T_e}) high frequency fluctuations between 300 and 400 kHz set in. The pre-ELM phases (between -2.1 and -0.1 ms relative to the ELM onset) are analyzed in detail by the ELM synchronized toroidal mode number histograms (Figs. 5 b and 5 d). The sign of the mode numbers indicates their rotation direction. Positive n represent a co-current (toroidal) or ion-diamagnetic (poloidal) propagation direction, whereas negative n indicate a counter-current (toroidal) or electron-diamagnetic (poloidal) propagation direction. At lower frequencies the core mode has a clear $n = +1, +2$ structure for both plasmas. The

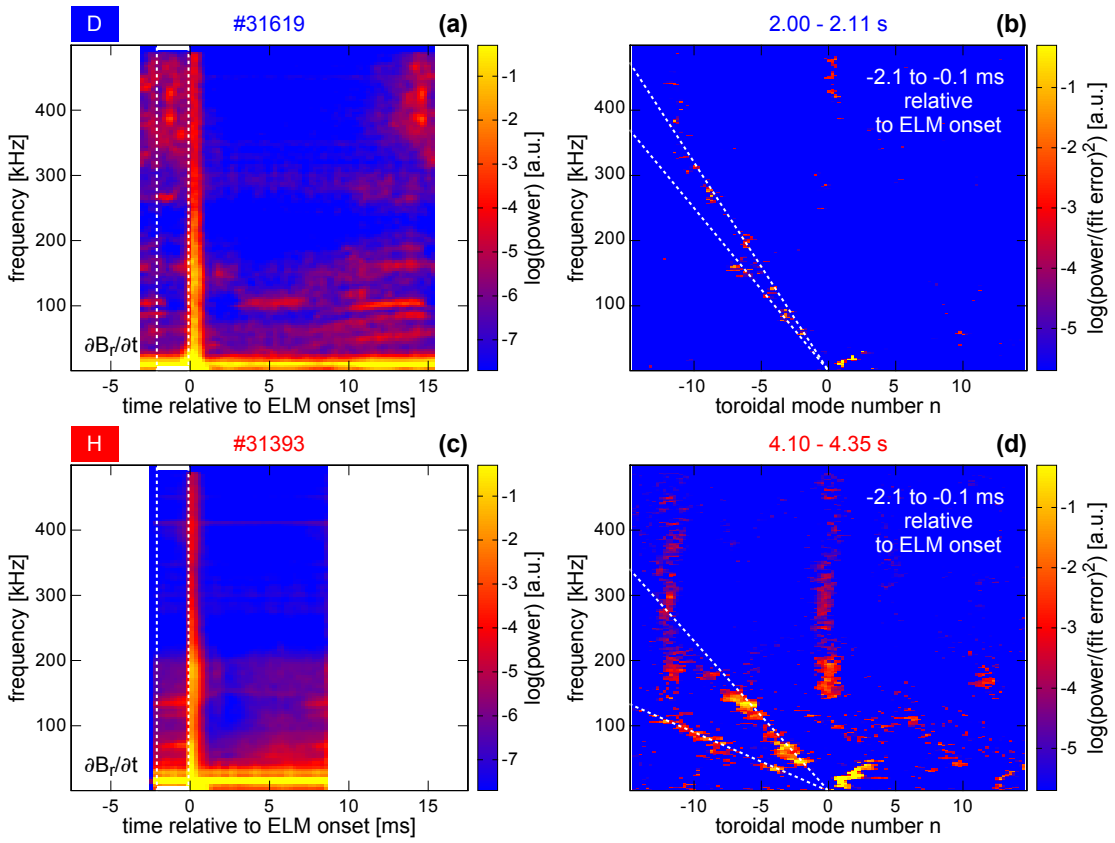

FIG. 5: Comparison of the magnetic fluctuations: ELM synchronized (a,c) frequency and (b,d) toroidal mode number histograms (determined between −2.1 and −0.1 ms relative to the ELM onset) for (a,b) D and (c,d) H. The white dashed lines in (a,c) indicate the time interval of the mode number determination and in (b,d) the two mode branches with different propagation velocity. Similar inter-ELM activity and corresponding toroidal structure can be seen in D and H. The different detected frequencies for similar n correspond to different rotation velocities relative to the lab frame.

higher frequency range shows two mode branches with negative n for D and H as it has been found previously in a D discharge[30]. These are indicated by the white dashed lines, which inclination represent the rotation velocity relative to the lab frame. The different inclination means that the two branches rotate at different velocities. The shallower slopes of the branches in H in comparison to D indicate a lower rotation velocity. This can be explained by the different n_e profile in H, since the E×B flow at the edge is proportional to $\nabla p_i/(e \cdot n_i)$. Assuming $\nabla n_i/n_i \approx \nabla n_e/n_e$, the shallower ∇n_e in H leads to a lower background E × B velocity.

It can be seen that the branches have similar structure in both main ion species. At medium frequencies n is in the region of -3 to -8. Consistent with the more broadband ELM synchronized frequency histograms in H, the measured n have less distinct peaks in the mode number range than in D. The high frequency fluctuations are related to n in the region of -11 in both main ion species.

The comparison of the pre-ELM structure of $\partial B_\mathrm{r}/\partial t$ reveals similar n for both main ion species, which also supports that similar instabilities are present in these plasmas. The detected rotation velocities differ, since the E $\times$ B flow velocity is affected by the shallower density gradient in H.

IV. HELIUM PLASMAS

For further comparison to another main ion species, ^{4}He plasmas were performed. Again a match of the pedestal n_e and T_e to the D and H references (see Section III A) was envisaged. However, due to the two electrons provided by a ^{4}He atom to the plasma, the main ion density (n_i) was lower in comparison to hydrogenic species at similar n_e.

In ^{4}He several operational boundaries at ASDEX Upgrade have to be taken into account. For the density control only a small pumping rate by the turbomolecular pumps are available. This issue can be overcome by applying argon frosting[31]. It was decided to operate the NBI with H for these experiments, because ^{4}He NBI would suffer from a significant reduction of available P_heat and no CXRS measurements for T_i would be possible. According to these operational limits, plasmas with a ^{4}He concentration in the region of 80 % of the ion density were performed. Approximately 17 % H content is caused by the NBI and a 3 % D concentration is due to residual gas released from the wall.

A. Inter-ELM pedestal evolution

In comparison to the D and H discharges higher n_e pedestals are present in this period (Fig. 6) but W_MHD, f_ELM and relative ΔW_MHD are comparable to the D discharge. In Fig. 7 the evolution of ∇n_e, ∇T_e and ∇T_i at radial positions close to the separatrix (ρ_{pol} 0.98, 0.99) are shown. Similar recovery phases as in the hydrogenic plasmas are identified. Again n_e, respectively ∇n_e recovers faster than ∇T_e. Remarkably, ∇T_i does not follow the evolution

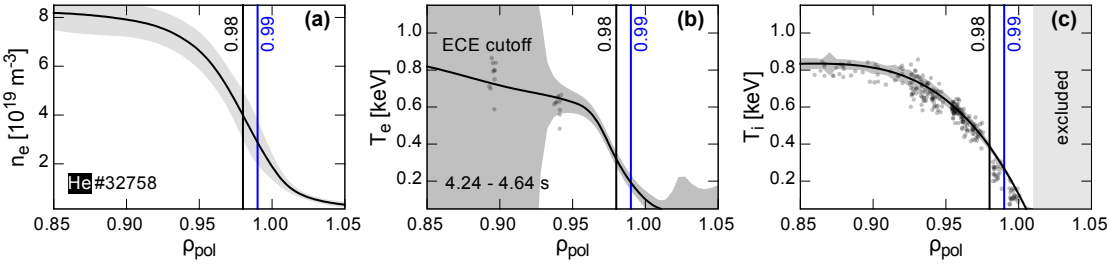

FIG. 6: Pedestal profiles in ^{4}He: (a) n_e, (b) T_e, (c) T_i, averaged between -2 and -1 ms relative to the ELM onset. The pedestal top n_e is roughly 50 % higher than in the hydrogenic species (see Fig. 1), leading to a cutoff of the ECE inside $\rho_{pol} = 0.95$.

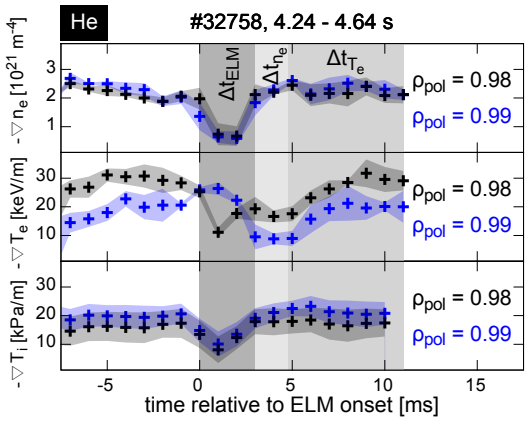

FIG. 7: Temporal evolution of the pedestal gradients in ^{4}He: ∇n_e, ∇T_e and ∇T_i at two positions in the pedestal ($\rho_{pol} = 0.98$, 0.99). The recovery of ∇n_e and ∇T_i take place on similar timescales (Δt_{n_e}), whereas ∇T_e is established later in the ELM cycle (Δt_{T_e}).

of ∇T_e but rather is re-established after Δt_{n_e}, which is the recovery timescale of n_e. Such a behaviour was also suggested by the comparison of the neoclassically estimated current in the pedestal (using T_i equal to T_e) and the current in the pedestal reconstructed from magnetic measurements[26], because the neoclassically estimated current evolves slower than the reconstructed one. More recently, the recovery behaviour of T_i has also been investigated in D plasmas, where impurities were puffed for fast T_i measurements[32]. It has also been found that the T_i pedestal recovers on similar time as the n_e pedestal.

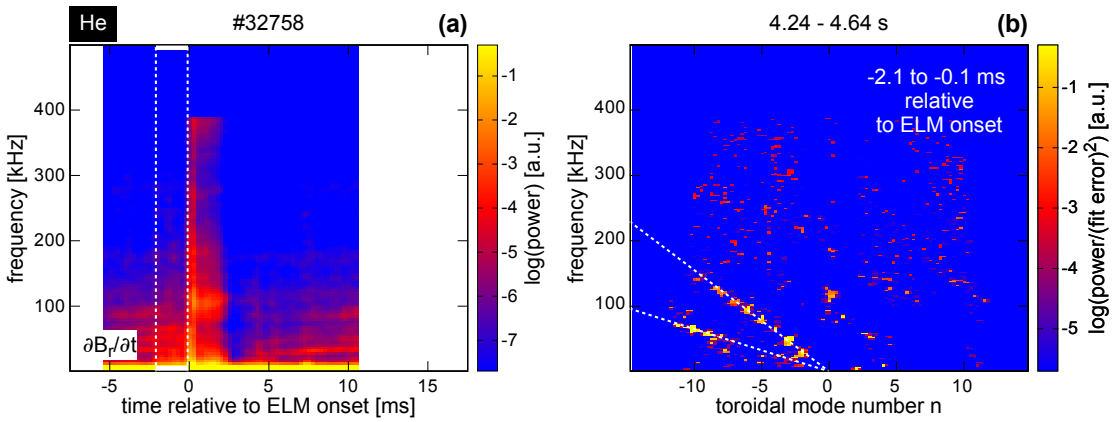

FIG. 8: Comparison of the magnetic fluctuations: ELM synchronized (a) frequency and (b) toroidal mode number histograms (determined between −2.1 and −0.1 ms relative to the ELM onset) for ^{4}He. The white dashed lines in (a) indicate the time interval of the mode number determination and in (b) the two mode branches with different propagation velocity. In comparison to D and H similar magnetic activity and n are found at lower detected frequencies owing to the lower propagation velocity relative to the lab frame.

B. Structure of pre-ELM magnetic fluctuations

As it can be seen in the ELM synchronized frequency histograms there is much less medium and high frequency magnetic activity (100 to 400 kHz, Fig. 8 a) than in the investigated cases of D and H. Also the frequency of an acting core mode is lower in ^{4}He. Both are indications that the rotation velocities are lower in this case. The low core rotation can be explained by the lower NBI momentum input than e.g. in H (less NBI sources), whereas a lower poloidal edge rotation can be explained by a change in the $\nabla p_\mathrm{i}/(e \cdot n_\mathrm{i})$ term.

During Δt_{n_e} a phase with very low magnetic activity is present, similar to the one observed in the hydrogenic plasmas. Later on in the ELM cycle well defined frequency bands develop, which last till the onset of the next ELM.

Analyzing the pre-ELM (determined between −2.1 and −0.1 ms relative to the ELM onset) toroidal structure (Fig. 8 b) two mode branches are found, similar to the one in D and H. The contributing mode numbers are well defined and in the range of n −2 to −11. As indicated by the white dashed lines the propagation velocities relative to the lab frame are lower than in the hydrogenic plasmas. This is in line with a lower rotation of the plasma owing to the previously discussed arguments. In summary, clear evidence is found that the

same kind of instabilities as in hydrogenic plasmas are also present and dominant in the pedestal of ^{4}He plasmas with ELMs.

V. SUMMARY AND DISCUSSION

Pedestal matching experiments between D, H and ^{4}He plasmas were performed to compare the pedestal structure, stability and inter-ELM evolution. The overall behaviour of these discharges was different in the sense that different energy as well as particle confinement is observed. In H due to lower particle confinement a shallower ∇n_e is found and a factor of approximately 2 higher heat flux through the pedestal is estimated in comparison to D. In ^{4}He due to the higher plasma dilution (lower n_i) the n_e at the pedestal top is roughly 50 % larger than for the hydrogenic references with similar W_MHD and T_e pedestal profiles.

The analyses of the inter-ELM n_e and T_e profile evolutions showed similar sequences in the pedestal recovery for D, H and ^{4}He. After the ELM crash the n_e pedestal recovers first, then the T_e pedestal recovers. In ^{4}He detailed studies on the inter-ELM recovery of the T_i pedestal were made. These show that T_i recovers on the same timescale as n_e, as suggested previously[26] and also observed in D plasmas with impurity seeding[32]. The magnetic activity throughout the ELM cycle is comparable in all investigated main ions species. After the ELM, which causes large magnetic fluctuations a phase with very low activity is found, which duration corresponds to the recovery of the n_e pedestal. Later on the magnetic fluctuations with a sometimes well defined band structure set in, which continue till the next ELM crash. These have similar n in the range of -3 to -8 in all presented cases. When the pedestals of n_e and T_e are recovered, fluctuations with n in the region of n -10 to -11 set in. Furthermore, two mode branches with different propagation velocities relative to the lab frame can be identified. Comparing the different main ion species, changes in the edge profiles impact the E $\times$ B flow which can explain the different propagation velocity relative to the lab frame.

In conclusion, the experimental observations suggest that the pedestal stability can be sufficiently described by PB theory in the investigated hydrogenic species plasmas. The non-linear phase of the ELM crash could be affected since the ELM losses vary when the main isotope species is exchanged. The inter-ELM pedestal recovery behaviour as well as

the identified magnetic signature and structure point into the direction that the sequence of dominant mechanisms in the pedestal evolution proceeds independently of the main ion species.

VI. ACKNOWLEDGEMENT

F. M. Laggner is a fellow of the Friedrich Schiedel Foundation for Energy Technology. This work has been carried out within the framework of the EUROfusion Consortium and has received funding from the Euratom research and training programme 2014-2018 under grant agreement No 633053. The views and opinions expressed herein do not necessarily reflect those of the European Commission.

REFERENCES

[1]R. Aymar, P. Barabaschi, Y. Shimomura, and the ITER Team, Plasma Physics and Controlled Fusion **44**, 519 (2002).

[2]H. Biglari, P. H. Diamond, and P. W. Terry, Physics of Fluids B-Plasma Physics **2**, 1 (1990).

[3]J. W. Connor and H. R. Wilson, Plasma Physics and Controlled Fusion **42**, R1 (2000).

[4]D. Boucher and V. Mukhovatov, Plasma Physics and Controlled Fusion **38**, 1225 (1996).

[5]Y. R. Martin, T. Takizuka, and ITPA CDBM H-mode Threshold Database Working Team, 11th Iaea Technical Meeting on H-Mode Physics and Transport Barriers **123**, 012033 (2008).

[6]F. Ryter, M. Cavedon, T. Happel, R. M. McDermott, E. Viezzer, G. D. Conway, R. Fischer, B. Kurzan, T. Putterich, G. Tardini, M. Willensdorfer, and A. U. Team, Plasma Physics and Controlled Fusion **58**, 014007 (2016).

[7]M. Bessenrodt-Weberpals, F. Wagner, O. Gehre, L. Giannone, J. V. Hofmann, A. Kallenbach, K. McCormick, V. Mertens, H. D. Murmann, F. Ryter, B. D. Scott, G. Siller, F. X. Soldner, A. Stabler, K. H. Steuer, U. Stroth, N. Tsois, H. Verbeek, and H. Zoohm, Nuclear Fusion **33**, 1205 (1993).

[8]F. Wagner and U. Stroth, Plasma Physics and Controlled Fusion **35**, 1321 (1993).

[9]H. Urano, T. Takizuka, M. Kikuchi, T. Nakano, N. Hayashi, N. Oyama, and Y. Kamada, Physical Review Letters **109** (2012), 10.1103/PhysRevLett.109.125001.

[10]P. A. Schneider, L. B. Orte, A. Burckhart, M. G. Dunne, C. Fuchs, A. Gude, B. Kurzan, W. Suttrop, E. Wolfrum, and the ASDEX Upgrade Team, Plasma Physics and Controlled Fusion **57**, 014029 (2015).

[11]V. P. Bhatnagar, J. Lingertat, R. Barnsley, P. Breger, J. P. Christiansen, S. Clement, J. G. Cordey, S. J. Davies, J. K. Ehrenberg, L. G. Eriksson, G. M. Fishpool, P. J. Harbour, L. D. Horton, J. Jacquinot, H. J. Jackel, K. Lawson, C. G. Lowry, C. F. Maggi, G. F. Matthews, R. D. Monk, D. P. O'Brien, V. V. Parail, E. Righi, G. Saibene, R. Sartori, B. Schunke, A. C. C. Sips, M. F. Stamp, D. F. H. Start, and K. Thomsen, Nuclear Fusion **39**, 353 (1999).

[12]A. Scarabosio, C. Fuchs, A. Herrmann, E. Wolfrum, and A. U. Team, Journal of Nuclear Materials **415**, S877 (2011).

[13]C. McDonald, J. G. Cordey, E. Righi, F. Ryter, G. Saibene, R. Sartori, B. Alper, M. Becoulet, J. Brzozowski, I. Coffey, M. de Baar, P. de Vries, K. Erents, W. Fundamenski, C. Giroud, I. Jenkins, A. Loarte, P. J. Lomas, G. P. Maddison, J. Mailloux, A. Murari, J. Ongena, J. Rapp, R. A. Pitts, M. Stamp, J. Strachan, W. Suttrop, and JET EFDA Contributors, Plasma Physics and Controlled Fusion **46**, 519 (2004).

[14]H. Urano, T. Takizuka, N. Aiba, M. Kikuchi, T. Nakano, T. Fujita, N. Oyama, Y. Kamada, N. Hayashi, and the JT-60 Team, Nuclear Fusion **53**, 083003 (2013).

[15]H. Urano, Nuclear Fusion **54**, 116001 (2014).

[16]E. Wolfrum, E. Viezzer, A. Burckhart, M. G. Dunne, P. A. Schneider, M. Willensdorfer, E. Fable, R. Fischer, D. Hatch, F. Jenko, B. Kurzan, P. Manz, S. K. Rathgeber, and the ASDEX Upgrade Team, Nuclear Fusion **55**, 053017 (2015).

[17]M. Willensdorfer, G. Birkenmeier, R. Fischer, F. M. Laggner, E. Wolfrum, G. Veres, F. Aumayr, D. Carralero, L. Guimarais, B. Kurzan, and the ASDEX Upgrade Team, Plasma Physics and Controlled Fusion **56**, 025008 (2014).

[18]A. Mlynek, M. Reich, L. Giannone, W. Treutterer, K. Behler, H. Blank, A. Buhler, R. Cole, H. Eixenberger, R. Fischer, A. Lohs, K. Luddecke, R. Merkel, G. Neu, F. Ryter, D. Zasche, and the ASDEX Upgrade Team, Nuclear Fusion **51**, 043002 (2011).

[19]W. Suttrop, A. G. Peeters, the ASDEX Upgrade Team, and the NBI group, "Practical limitations to plasma edge electron temperature measurements by radiometry of electron

cyclotron emission," Tech. Rep. (1996).

[20]R. Fischer, C. J. Fuchs, B. Kurzan, W. Suttrop, E. Wolfrum, and the ASDEX Upgrade Team, Fusion Science and Technology **58**, 675 (2010).

[21]S. K. Rathgeber, L. Barrera, T. Eich, R. Fischer, B. Nold, W. Suttrop, M. Willensdorfer, E. Wolfrum, and A. U. Team, Plasma Physics and Controlled Fusion **55**, 025004 (2013).

[22]B. Kurzan, H. Murmann, H. Salzmann, and the ASDEX Upgrade Team, Review of Scientific Instruments **72**, 1111 (2001).

[23]E. Viezzer, T. Putterich, R. Dux, R. M. McDermott, and the ASDEX Upgrade Team, Rev Sci Instrum **83**, 103501 (2012).

[24]M. Cavedon, T. Putterich, E. Viezzer, R. M. Dux, B. Geiger, R. McDermott, H. Meyer, U. Stroth, and the ASDEX Upgrade Team, In preparation for Review of Scientific Instruments (2016).

[25]M. Dunne, L. Frassinetti, M. N. A. Beurskens, M. Cavedon, S. Fietz, R. Fischer, L. Giannone, G. T. A. Huijsmans, B. Kurzan, F. M. Laggner, P. J. McCarthy, R. M. McDermott, G. Tardini, E. Viezzer, M. Willensdorfer, E. Wolfrum, E. M. Team, and the ASDEX Upgrade Team, Accepted in Plasma Physics and Controlled Fusion (2016).

[26]M. G. Dunne, P. J. McCarthy, E. Wolfrum, R. Fischer, L. Giannone, A. Burckhart, and the ASDEX Upgrade Team, Nuclear Fusion **52**, 123014 (2012).

[27]F. M. Laggner, E. Wolfrum, M. Cavedon, F. Mink, E. Viezzer, M. G. Dunne, P. Manz, H. Doerk, G. Birkenmeier, R. Fischer, S. Fietz, M. Maraschek, M. Willensdorfer, F. Aumayr, and the ASDEX Upgrade Team, Plasma Physics and Controlled Fusion **58**, 065005 (2016).

[28]A. Burckhart, E. Wolfrum, R. Fischer, K. Lackner, H. Zohm, and the ASDEX Upgrade Team, Plasma Physics and Controlled Fusion **52**, 105010 (2010).

[29]L. Horvth, P. Z. Poloskei, G. Papp, M. Maraschek, K. H. Schuhbeck, G. I. Pokol, the EUROfusion MST1 Team, and the ASDEX Upgrade Team, Plasma Physics and Controlled Fusion **57**, 125005 (2015).

[30]F. Mink, E. Wolfrum, M. Maraschek, H. Zohm, L. Horvth, F. M. Laggner, P. Manz, E. Viezzer, U. Stroth, and the ASDEX Upgrade Team, Plasma Physics and Controlled Fusion **58**, 125013 (2016).

[31]M. R. Wade, D. L. Hillis, J. T. Hogan, M. A. Mahdavi, R. Maingi, W. P. West, N. H. Brooks, K. H. Burrell, R. J. Groebner, G. L. Jackson, C. C. Klepper, G. Laughon, M. M.

Menon, and P. K. Mioduszewski, Physical Review Letters **74**, 2702 (1995).

[32]M. Cavedon and the ASDEX Upgrade Team, In preparation for Plasma Physics and Controlled Fusion (2016).